Flight Dynamics of the Boomerang, Part 1: Fundamental Analysis

Akira Azuma*
University of Tokyo, Kawasaki 212-0021, Japan
Goro Beppu† and Hiroaki Ishikawa‡
Tokai University, Hiratsuka 259-1292, Japan
and
Kunio Yasuda§
Nihon University, Funabashi 274-8501, Japan

Equations of motion for boomerang flight dynamics are presented in strictly nonlinear form and solved numerically for a typical returning boomerang. The solution shows that the motion consists of both long- and short-period oscillations. The long-period oscillation originates from the exchange of potential (altitude) energy with kinetic energy mainly derived from the forward motion and the spinning motion, the latter of which is accelerated by the autorotation when the angle of attack of an apparent disk of blade rotation increases. The short-period oscillation is due to an asymmetry in the aerodynamic moment related to a large reversed-flow region and a stalled region due to high-advance-ratio flight, and a large moment of inertia or a small Lock number that is an order of magnitude smaller than that of a helicopter blade. The return flight is realized by the centripetal component of the aerodynamic force acting on the apparent disk that is tilted inwardly from the described asymmetric moment and the resulting gyro effect of the spinning motion.

Nomenclature

a	=	acceleration at any position r in body frame, $(a_x, a_y, a_z)^T$
C^A	=	aerodynamic force coefficient, $(C_x^A, C_y^A, C_z^A)^T$, equal to $F^A/\frac{1}{2}\rho(R\Omega)^2 S$
C^G	=	gravity force coefficients, $(C_x^G, C_y^G, C_z^G)^T$, equal to F^G/mg
C_M^A	=	aerodynamic moment coefficient, $(C_{M,x}^A, C_{M,y}^A, C_{M,z}^A)^T$, equal to $M^A/\frac{1}{2}\rho(R\Omega)^2 RS$
d	=	drag of blade element
E	=	total energy
E^K	=	kinetic energy $= E^L + E^R$
E^L	=	kinetic energy given by linear or translational motion
E^P	=	potential energy given by altitude
E^R	=	kinetic energy given by rotational motion
F^A	=	total aerodynamic force acting on boomerang, $(F_x^A, F_y^A, F_z^A)^T$
F_j^A	=	aerodynamic force acting on jth blade, $(F_{x,j}^A, F_{y,j}^A, F_{z,j}^A)^T$
F^I	=	inertial force in body frame, $(F_x^I, F_y^I, F_z^I)^T$
F^G	=	gravity force of boomerang, $(F_x^G, F_y^G, F_z^G)^T$
g	=	gravity acceleration
J	=	inertial tensor, $(I_x, I_y, I_z, J_{xy}, J_{xz})^T$
J_j	=	moment and product of inertia of jth blade, $(I_{\xi,j}, I_{\eta,j}, I_{\varsigma,j}, J_{\xi\eta,j}, J_{\xi\varsigma,j})^T$
K_I	=	unit vector along Z_I axis
k	=	unit vector along z axis; $k = 1$ for normal flow region, $k = -1$ for reversed flow region
ℓ	=	lift of blade element
ℓ_c	=	longitudinal distance of midchord line from c.g. point
ℓ_j	=	length of jth blade
M^A	=	total aerodynamic moment acting on boomerang, $(M_x^A, M_y^A, M_z^A)^T$
M_j^A	=	aerodynamic moment acting on jth blade, $(M_{x,j}^A, M_{y,j}^A, M_{z,j}^A)^T$
M^G	=	gravity moment of boomerang, $(M_x^G, M_y^G, M_z^G)^T$
M^I	=	inertial moment in body frame, $(M_x^I, M_y^I, M_z^I)^T$
m	=	mass of boomerang
m_j	=	mass of jth blade
m_η	=	feathering moment of blade element
R	=	reference radius
R	=	position vector of the origin of body frame in inertial frame, $(X_I, Y_I, Z_I)^T$
Re	=	Reynolds number at $\eta_j = (\frac{3}{4})\ell_j$
r	=	any position vector in body frame, $(x, y, z)^T$
$r_{\text{ac},j}$	=	position vector of aerodynamic center at blade root, $(x_{\text{ac},j}, 0, 0)^T$
r_j^A	=	position vector of the aerodynamic center at spanwise station η_j
r_j^I	=	position of an element considering the inertial force and moment in body frame
S	=	reference area
T_0, T_n, T, T_I, T_j	=	coordinate transformation matrices
t	=	time
U	=	translational velocity of the origin of body frame and nonslipping frame expressed in inertial frame, $(\dot{X}, \dot{Y}, \dot{Z})^T$, equal to $\dot{R}$
U_p	=	upward inflow through the rotor, $V\sin(\Theta - \gamma) - \bar{v}$
u	=	linear velocity of body frame expressed in body frame, $(u_x, u_y, u_z)^T$
V	=	translational speed in inertial space, $\sqrt{(\dot{X}_I^2 + \dot{Y}_I^2 + \dot{Z}_I^2)}$
v	=	velocity at any position r in body frame, $(v_x, v_y, v_z)^T$
v_j	=	velocity at the aerodynamic center of jth blade, $(v_{x,j}, v_{y,j}, v_{z,j})^T$
w	=	relative flow velocity of blade element

(X, Y, Z)	=	nonspinning or nonslipping frame
(X_A, Y_A, Z_A), (X_B, Y_B, Z_B)	=	intermediate frames
(X_I, Y_I, Z_I)	=	inertial frame
(X_0, Y_0, Z_0)	=	body frame at initial state
(X_1, Y_1, Z_1), (X_2, Y_2, Z_2)	=	intermediate frames
(x, y, z)	=	body frame
(x_1, y_1, z_1), (x_2, y_2, z_2), (x_3, y_3, z_3)	=	intermediate frames
α	=	angle of attack of blade element
α_{stall}	=	stalling angle of attack
β_j	=	coning angle, rotation about x_2 axis
γ	=	folding angle or joint angle of two blades $= \Lambda_2 - \Lambda_1$; climbing angle, $= \tan^{-1}(\dot{Z}_I/\dot{X}_I)$
$\Delta\theta_t$	=	blade twist, positive for washin
$\Delta\Lambda$	=	differential angle, $\pi - \gamma$
δ	=	differential angle showing tennis racket effect
$\boldsymbol{\eta}$	=	unit vector along η axis
Θ	=	pitching angle of nonslipping frame, rotation about Y_A axis
θ	=	feathering angle, rotation about Y_1 axis
θ_j	=	pitch angle, rotation about y_3 axis
Λ_j	=	sweep angle, rotation about z_1 axis $-\pi/2$
λ	=	rotation about Z axis, defined by Eq. (3a)
$\bar{\lambda}$	=	inflow ratio
μ	=	advance ratio
$(\xi_j, \eta_j, \varsigma_j)$	=	blade frame of jth blade
$(\bar{\xi}_j, \bar{\eta}_j, \bar{\varsigma}_j)^T$	=	center of gravity
ρ	=	air density
$\boldsymbol{\upsilon}$	=	induced velocity, $(0, 0, -\bar{\upsilon})^T$
$\bar{\upsilon}$	=	mean induced velocity, $|\boldsymbol{\upsilon}|$
Φ	=	rolling angle or bank angle of nonspinning axis, rotation about X_B axis
ϕ	=	flapping, rotation about X_2 axis
Ψ	=	yawing angle of nonslipping frame, rotation about Z axis
ψ	=	spin or rotation about Z_0 axis
Ω	=	initial spin rate, $\dot{\psi}(t=0)$, equal to $r(t=0)$ about z axis
$\boldsymbol{\omega}$	=	angular velocity, $(p, q, r)^T$
$\boldsymbol{\omega}_A, \boldsymbol{\omega}_B, \boldsymbol{\omega}_C$	=	rate of Euler's angle in respective frames, $(0, 0, \dot{\Psi})^T$, $(0, \dot{\Theta}, 0)^T$, and $(\dot{\Phi}, 0, 0)^T$
$\boldsymbol{\omega}_n$	=	angular velocity of nonslipping frame, $(p_n, q_n, r_n)^T$
$\boldsymbol{\omega}_1, \boldsymbol{\omega}_2, \boldsymbol{\omega}_3$	=	rate of Euler's angle of respective frames, $(0, 0, \dot{\psi})^T$, $(0, \dot{\theta}, 0)^T$, and $(\dot{\phi}, 0, 0)^T$

Subscript

|		
0	=	initial state

Introduction

A BOOMERANG is one of the oddest devices ever to serve as a weapon or plaything. A boomerang used as an offensive weapon can fly along a more or less straight horizontal line for a long distance and strike an object with amazing force. A boomerang used as a plaything is usually a returning boomerang whose flight path returns to the thrower. Boomerangs vary markedly in their shape, size, and weight.[1] The boomerang is said to have originated among the aboriginal inhabitants of Australia. A typical boomerang has two blades arranged in a plane and that are connected to each other diagonally at the respective blade ends, and the cross-sectional profile of the blade is, like the airplane wing profile, a lens-shaped profile throughout its whole length. That is, the profile is thin and more convex on one side than the other side, which is mostly flat. The returning boomerang is smaller than the weapon boomerang and is usually 0.3–0.8 m in length and 0.1–0.4 kg in mass.

On launching, a boomerang is usually held almost vertically by the tip of one of the blades with the flat side away from the thrower.

The arm of the thrower is brought behind the shoulder. On take-off, the boomerang is thrown toward the horizon or in a slightly upward direction with forward snapping when the thrower's arm is fully stretched forward. In this way, the boomerang starts its flight with a forward speed and a rotational or spinning motion. At first the boomerang just seems to fly away, but it soon swerves to the left (right) for a right- (or left-) handed thrower, and also upward, traverses a wide loop, approaches the thrower, and may descend somewhere near the thrower's feet, or describe a second, smaller, loop before reaching the ground. Generally, the rolling or bank angle of the boomerang's plane of rotation gradually decreases so that it may be nearly horizontal at the end of the flight.[2]

Many experimental flight tests of various boomerangs, mostly returning boomerangs, have been performed. Typical examples are reported by, for example, Hess,[1,2] King,[3] and Vos.[4] Flight paths of our experimental boomerangs, as shown in Fig. 1a, were recorded by two video or movie cameras, as well as still cameras, by photographic time exposures of traces made by a light bulb attached to the boomerang. Then the three-dimensional flight paths of the boomerang were analyzed along with the time variations of linear and angular velocities. Figure 1b shows a typical recorded flight path. However, because these results were obtained with poor resolution, numerical calculations based on the theoretical analysis were required to conduct detailed analyses of the flight for various initial conditions and geometrical shapes of a boomerang.

Hess[2] presented a theoretical analysis of boomerang aerodynamics and motion together with various numerical calculations and experimental flight tests for a variety of geometrical shapes and takeoffs or initial conditions. However, in his analysis, the equations of boomerang motion are smoothed such that variations of physical quantities within one spin period are disregarded. Furthermore, the boomerang is replaced by a circular disk, which is a continuous

Lithic cell
Socket
Light-emittg diode

Pipe made of acrylic resin
14mm
30mm
Socket
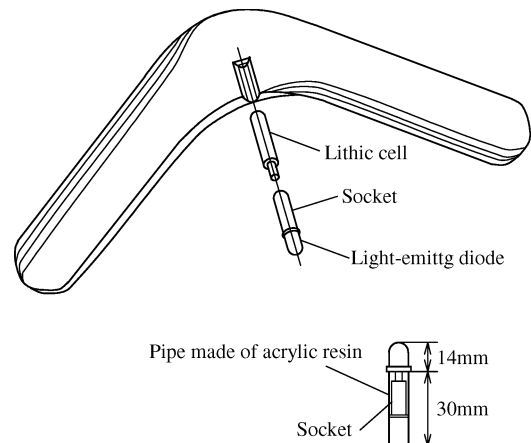
a) Flight model with luminous device
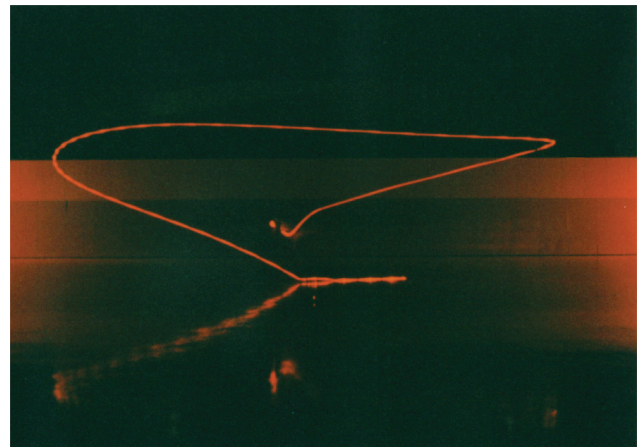
b) Example of flight path recorded

Fig. 1 Model used for numerical calculation and flight tests.

distribution of hypothetical winglets, each of which is simulated by a nonrotating, rigid, porous wing having the same planform. Thus, the aerodynamic forces and moments acting on the boomerang are obtained by a steady, linearized, porous lifting surface theory under the assumption of small angle of attack.

In the present paper the following assumptions will be introduced for simplicity of theoretical treatment: 1) The boomerang is a rigid body without any elastic deformation during the flight. 2) The blade pitch or feathering angle is presented by an aerodynamic pitch angle of the zero-lift line of the airfoil with respect to a reference plane or a rotational plane. 3) The induced velocity is homogeneous over the rotational plane, and its magnitude is decided from the momentum balance with respect to the time-averaged aerodynamic thrust acting on the boomerang over one period of rotation. 4) The analysis may be derived from blade element theory based on the quasi-steady lifting-line theory. From the second assumption, the blade pitch setting of a two-bladed boomerang at the blade root is considered to be a summation of the collective pitch angle of zero-lift line of one blade and that of the other blade. Then zero twist means that the pitch is flat (or zero). The third assumption is appropriate because the boomerang is moving with such a high speed, or with a large advance ratio μ ($0.5 < \mu < 1.5$), that the effect of the nonuniformity of induced velocity on the inflow into the rotational plane is small.

Theoretical Analysis

Coordinate Systems

Let us consider two right-handed Cartesian coordinate systems or frames: a body frame (x, y, z) fixed to a boomerang and the frame at its initial state (X_0, Y_0, Z_0), both of which frames are fixed to the center of gravity of the boomerang. The coordinate transformation $\boldsymbol{T}_0$ between the two frames is given by three successive transformations through Euler's angles, such as spin rotation ψ, feathering θ, and flapping ϕ. The detailed expressions of the transformation matrix $\boldsymbol{T}_0$ is

$$\boldsymbol{T}_0 = \begin{pmatrix} \cos\theta\cos\psi & \cos\theta\sin\psi & -\sin\theta \\ \begin{matrix} -\cos\phi\sin\psi \\ +\sin\phi\sin\theta\cos\psi \end{matrix} & \begin{matrix} \cos\phi\cos\psi \\ +\sin\phi\sin\theta\sin\psi \end{matrix} & \sin\phi\cos\theta \\ \begin{matrix} \sin\phi\sin\psi \\ +\cos\phi\sin\theta\cos\psi \end{matrix} & \begin{matrix} -\sin\phi\cos\psi \\ +\cos\phi\sin\theta\sin\psi \end{matrix} & \cos\phi\cos\theta \end{pmatrix} \tag{1}$$

At takeoff, the boomerang is driven by a human hand with an initial angular velocity $\boldsymbol{\omega}_0 = \boldsymbol{\omega}(t=0) = (p_0, q_0, r_0)^T$ and an initial linear velocity $\boldsymbol{u}_0 = \boldsymbol{u}(t=0) = (u_{x,0}, u_{y,0}, u_{z,0})^T$. The boomerang flies freely in the atmosphere under the gravity force. Usually, both the initial spin rate r_0 and the initial speed $|u_0|$ are considered to be appreciably larger than any other quantity at the initial stage, $t = 0$.

When the rate of Euler's angles $\dot\psi, \dot\theta$, and $\dot\phi$ is used, the angular velocity of the body frame $\boldsymbol{\omega} = (p, q, r)^T$ and its inverse form are given by

$$p = \dot\phi - \dot\psi\sin\theta \tag{2a}$$

$$q = \dot\theta\cos\phi + \dot\psi\cos\theta\sin\phi \tag{2b}$$

$$r = -\dot\theta\sin\phi + \dot\psi\cos\theta\cos\phi \tag{2c}$$

$$\dot\psi = q\sin\phi/\cos\theta + r\cos\phi/\cos\theta \tag{2d}$$

$$\dot\theta = q\cos\phi - r\sin\phi \tag{2e}$$

$$\dot\phi = p + q\sin\phi\tan\theta + r\cos\phi\tan\theta \tag{2f}$$

Let us further consider a nonspinning (or nonslipping) frame (X, Y, Z), the Z axis of which is coaxial with the z axis of the body frame and is free from the spinning motion of the boomerang. The nonspinning frame is obtained by rotating its Z axis with spinning speed of $-\dot\lambda$ with respect to the body frame. Thus, the nonspinning frame can be considered to be fixed to a flying disk in which the blades or the body frame are spinning. The matrix for transforming from the body frame to the nonspinning frame is given by $\boldsymbol{T}_n$, in

which λ is the azimuth angle of the body frame with respect to the nonspinning frame,

$$\lambda = \int_0^t (r - r_n)\,\mathrm{d}t \tag{3a}$$

where r_n is the angular velocity about the Z axis. The detailed expression of the matrix $\boldsymbol{T}_n$ is also given as

$$\boldsymbol{T}_n = \begin{pmatrix} \cos\lambda & -\sin\lambda & 0 \\ \sin\lambda & \cos\lambda & 0 \\ 0 & 0 & 1 \end{pmatrix} \tag{3b}$$

Thus, the matrix transformation from the initial frame (X_0, Y_0, Z_0) to the nonspinning frame (X, Y, Z) can be given by $\boldsymbol{T} = \boldsymbol{T}_n \cdot \boldsymbol{T}_0$.

The angular velocity in the nonspinning frame $\boldsymbol{\omega}_n$ is then given by $\boldsymbol{\omega}_n = (p_n, q_n, r_n)^T = \boldsymbol{T}_n \cdot \{\boldsymbol{\omega} - (0, 0, r - r_n)^T\}$. The detailed expression of this angular velocity is given by

$$p_n = p\cos\lambda - q\sin\lambda \tag{4a}$$

$$q_n = p\sin\lambda + q\cos\lambda \tag{4b}$$

$$r_n = r - \dot\lambda \tag{4c}$$

The angular rate of the Z axis of the nonspinning frame r_n can be determined to satisfy the following nonslipping condition: $u_Y = u_x\sin\lambda + u_y\cos\lambda = 0$ or $\lambda = -\tan(u_y/u_x)$. This further yields $\boldsymbol{r}_n = \boldsymbol{r} + \{(\dot u_y u_x - \dot u_x u_y)/(u_x^2 + u_y^2)\}$.

The nonspinning frame may also be defined another way from an inertial frame (X_I, Y_I, Z_I) fixed to the inertial space. The coordinate transformation from the inertial frame (X_I, Y_I, Z_I) to the nonspinning frame (X, Y, Z) with matrix $\boldsymbol{T}_I$ is performed by taking the following Euler's angles: yawing angle Ψ, pitching angle Θ, and rolling angle Φ. Unlike the convention in aircraft dynamics, the X_I and Z_I axes are directed backward and upward, respectively, at the initial state ($\Psi_0 = \Theta_0 = 0$), so that, in the present definition, the yawing and rolling angles used in aircraft dynamics are given by $-\Psi$ and $-\Phi$ respectively. The matrix $\boldsymbol{T}_I$ can be given by

$$\boldsymbol{T}_I = \begin{pmatrix} \cos\Theta\cos\Psi & \cos\Theta\sin\Psi & -\sin\Theta \\ \begin{matrix} -\cos\Phi\sin\Psi \\ +\sin\Phi\sin\Theta\cos\Psi \end{matrix} & \begin{matrix} \cos\Phi\cos\Psi \\ +\sin\Phi\sin\Theta\sin\Psi \end{matrix} & \sin\Phi\cos\Theta \\ \begin{matrix} \sin\Phi\sin\Psi \\ +\cos\Phi\sin\Theta\cos\Psi \end{matrix} & \begin{matrix} -\sin\Phi\cos\Psi \\ +\cos\Phi\sin\Theta\sin\Psi \end{matrix} & \cos\Phi\cos\Theta \end{pmatrix} \tag{5}$$

Then, the initial frame (X_0, Y_0, Z_0), which is equivalent to the nonspinning frame at $t = 0$, can be considered to be defined by the preceding successive transformations from the inertial frame (X_I, Y_I, Z_I) at the initial state, $(t = 0)$.

When the rate of Euler's angles $\dot\Psi, \dot\Theta$, and $\dot\Phi$ is used, the angular velocity of the nonspinning frame and its inverse form can be given by

$$p_n = \dot\Phi - \dot\Psi\sin\Theta \tag{6a}$$

$$q_n = \dot\Theta\cos\Phi + \dot\Psi\cos\Theta\sin\Phi \tag{6b}$$

$$r_n = -\dot\Theta\sin\Phi + \dot\Psi\cos\Theta\cos\Phi \tag{6c}$$

$$\dot\Psi = (p\sin\lambda + q\cos\lambda)\sin\Phi/\cos\Theta + r_n\cos\Phi/\cos\Theta \tag{6d}$$

$$\dot\Theta = (p\sin\lambda + q\cos\lambda)\cos\Phi - r_n\sin\Phi \tag{6e}$$

$$\dot\Phi = (p\cos\lambda - q\sin\lambda) + (p\sin\lambda + q\cos\lambda)\sin\Phi\tan\Theta$$
$$\quad + r_n\cos\Phi\tan\Theta \tag{6f}$$

It may be expressed in another way from Eqs. (4a–4b).

The linear velocity of the origin of the body frame (x, y, z), $\boldsymbol{u}$, can be related to that of the inertial frame $\boldsymbol{U} = \dot{\boldsymbol{R}} = (\dot X_I, \dot Y_I, \dot Z_I)^T$ as follows:

$$\boldsymbol{u} = \boldsymbol{T}_0 \cdot (\boldsymbol{T}_I)_0 \cdot \boldsymbol{U} \tag{7a}$$

or

$$U = (T_I)_0^{-1} \cdot T_0^{-1} \cdot u \tag{7b}$$

where the inverse transformation matrices $(T_I)_0^{-1}$ and T_0^{-1} are given by transposing the row of T_I at the initial state and T_0 with the column, respectively, because these matrices are unitary.

The velocity v and the acceleration a at a blade element given by the position vector $r = (x, y, z)^T$ in the body frame are then given by

$$v = u + \omega \times r \tag{8}$$

$$a = \dot{v} + \omega \times v = \dot{u} + \dot{\omega} \times r + \omega \times \dot{r} + \omega \times (u + \omega \times r) \tag{9}$$

The local velocity of the blade element $\dot{r}$ is usually discarded for rigid blades.

Geometrical Configuration of Blades

There are two assumptions made here: 1) The blades of a boomerang are composed of n blades (usually $n = 2$) arranged as shown in Fig. 2, in which only of two arms (blades $j = 1, 2$) are drawn. 2) The jth blade, typically represented by the line of aerodynamic center (a.c.) or feathering axis, the root of which is located at $r_{\mathrm{ac}, j} = (x_{\mathrm{ac}, j}, 0, 0)^T$ in the body frame, is arranged to have sweep angle Λ_j, coning angle β_j, and pitch angle θ_j, where the latter two, β_j and θ_j, are assumed small.

As shown in Fig. 2, we introduce another coordinate system or blade frame $(\xi_j, \eta_j, \varsigma_j)$ fixed to the jth blade. The ξ_j axis is normal to the η_j axis, which is fixed to the a.c. line. The ς_j axis is normal to the (ξ_j, η_j) plane. The origin of the coordinate system is located at the blade root $r_{\mathrm{ac}, j}$ in the (x, y, z) frame. The transformation is performed as follows: Shift the origin of the (x, y, z) frame by $r_{\mathrm{ac}, j}$, make the sweep angle $(\Lambda_j - \pi/2)$ or rotate about the z_1 axis, and take two further successive angular deflections: coning angle β_j, or rotation about x_2 axis, and pitch angle θ_j, or rotation about y_3 axis. Then the angular transformation from the body frame (x, y, z) to the blade frame $(\xi_j, \eta_j, \varsigma_j)$ can be given by the matrix T_j. The detailed expression of this matrix T_j is given as follows without the assumption of small β_j and θ_j:

$$T_j =$$

$$\begin{pmatrix} \begin{matrix} \sin \Lambda_j \cos \theta_j \\ + \cos \Lambda_j \sin \beta_j \sin \theta_j \end{matrix} & \begin{matrix} -\cos \Lambda_j \cos \theta_j \\ + \sin \Lambda_j \sin \beta_j \sin \theta_j \end{matrix} & -\cos \beta_j \sin \theta_j \\ -\cos \Lambda_j \cos \beta_j & \sin \Lambda_j \cos \beta_j & \sin \beta_j \\ \begin{matrix} \sin \Lambda_j \sin \theta_j \\ -\cos \Lambda_j \sin \beta_j \cos \theta_j \end{matrix} & \begin{matrix} -\cos \Lambda_j \sin \theta_j \\ -\sin \Lambda_j \sin \beta_j \cos \theta_j \end{matrix} & \cos \beta_j \cos \theta_j \end{pmatrix} \tag{10}$$
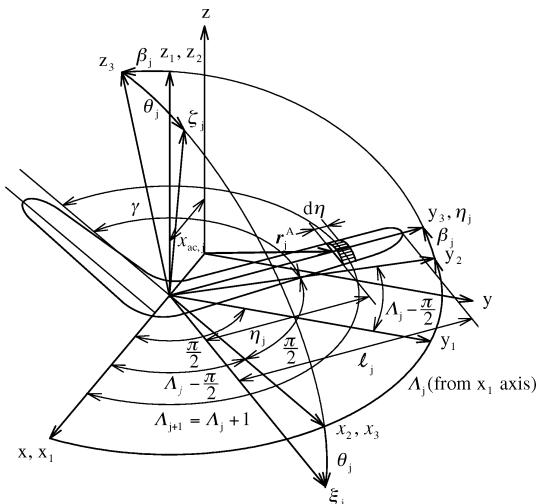
The azimuth angle of the advancing neighbor blade or $(j + 1)$th blade is given by $\Lambda_{j+1} = \Lambda_j + \gamma$, where γ is the joint angle between two neighbor blades.

External and Internal Forces and Moments

Aerodynamic Forces and Moments

A blade element of jth blade is represented by a position vector of the aerodynamic center at the spanwise station η_j as follows: $r_j^A = (x_{\mathrm{ac}}, 0, 0)^T + T_j^{-1} \cdot (0, \eta_j, 0)^T$. The velocity of the jth blade element v_j is given by the velocity at the origin $u = (u_x, u_y, u_z)^T$ and the velocity caused by the rotation ω given by Eqs. (2a–2c), $v_j = (v_{x,j}, v_{y,j}, v_{z,j})^T = u + \omega \times r_j^A$. The induced velocity v is assumed to be homogeneous and normal to the (x, y) plane and is given by $v = -k\bar{v} = (0, 0, -\bar{v})^T$, where k is a unit vector along the z axis and $\bar{v}$ will be determined later from the momentum and the aerodynamic force balance. Then the relative air velocity of the blade element in the $(\xi_j, \eta_j, \varsigma_j)$ frame, $w_j = (w_{\xi,j}, w_{\eta,j}, w_{\varsigma,j})^T$, which is defined to be positive to the direction of the respective axis, is given by $w_j = T_j \cdot (-v - v)$.

Refer to Fig. 3; if the blade has a spanwise twist $\Delta\theta_t(\eta)$, which is assumed small and positive for washin, then the angle of attack α of the blade element is given by $\alpha = \tan^{-1}(w_\varsigma/w_\xi) + \Delta\theta_t$.

The following assumptions are made: 1) The velocity component u_x and the angular velocity component r designated by $r \cong \dot{\psi}$ are very large in comparison to other components, so that the displacement of the aerodynamic center $x_{\mathrm{ac}, j}$, the velocity components $u_{y,j}$ and $u_{z,j}$, the induced velocity $\bar{v}$, the coning angle β_j, and the angular velocity components p and q may also be assumed small. 2) The quasi-steady aerodynamics based on the lifting-line theory may be applied. 3) The blade airfoil configuration is constant in the respective blade. 4) The blade element theory may be applied. Then the aerodynamic forces and moments acting on the jth blade can be given by F_j^A and M_j^A as follows:

$$F_j^A = \int_0^{\ell_j} \{(-\ell \sin \alpha + d \cos \alpha), 0, (\ell \cos \alpha + d \sin \alpha)\}^T \, d\eta \tag{11a}$$

$$M_j^A = \int_0^{\ell_j} \{(\ell \cos \alpha + d \sin \alpha)\eta, m_\eta, (\ell \sin \alpha - d \cos \alpha)\eta\}^T \, d\eta \tag{11b}$$

where $\ell = \frac{1}{2}\rho w^2 c C_\ell(\alpha)$, $d = \frac{1}{2}\rho w^2 c C_d(\alpha)$, and $m_\eta = \frac{1}{2}\rho w^2 c^2 C_m(\alpha)$ and where ℓ_j is the length of the jth blade.

The total force and moment acting on a boomerang are then given by

$$F^A = \sum_{j=1}^{n} \left(T_j^{-1} \cdot F_j^A\right) \tag{12a}$$

$$M^A = \sum_{j=1}^{n} \left\{T_j^{-1} \cdot M_j^A + r_{\mathrm{ac}, j} \times \left(T_j^{-1} \cdot F_j^A\right)\right\} \tag{12b}$$

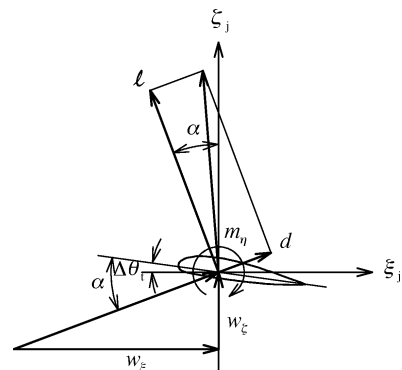Fig. 2 Blade frame (ξ_j, η_j, ζ_j) defined in body frame (x, y, z).

Fig. 3 Aerodynamic force and moment acting on a blade element.

The induced velocity $\bar{v}$ is determined from the momentum balance with the aerodynamic force as follows:

$$\bar{v} = \frac{1}{2\pi} \int_0^{2\pi} \left\{ \frac{F_z^A}{2\rho S \sqrt{u_x^2 + (u_z - \bar{v})^2}} \right\} d\psi$$

where iterations must be performed to obtain $\bar{v}$ by assuming an initial value such as $\bar{v} = 0$, and where the integration means taking the mean value within one rotation.

Gravity Force and Moment

By the specification that the gravity acceleration $\boldsymbol{g} = g\boldsymbol{K}_I$ is directed to the Z_I axis, where $\boldsymbol{K}_I$ is a unit vector along the Z_I axis, the gravity force $\boldsymbol{F}^G$ is given by

$$\boldsymbol{F}^G = \boldsymbol{T}_0 \cdot (\boldsymbol{T}_I)_0 \cdot (-m\boldsymbol{g}) = -mg\boldsymbol{T}_0 \cdot (\boldsymbol{T}_I)_0 \cdot \boldsymbol{K}_I \qquad (13a)$$

where $(\boldsymbol{T}_I)_0$ is the matrix $\boldsymbol{T}_I$ at $t = 0$ and m is the total mass of the boomerang. Because the origin of the (x, y, z) frame is located on the c.g., there is no gravitational moment acting on the boomerang at the c.g. point,

$$\boldsymbol{M}^G = 0 \qquad (13b)$$

Inertial Force and Moment

Let us consider elemental inertial force and moment acting on a blade element at a position $\boldsymbol{r} = \boldsymbol{r}_j^I$ where, as can be seen from Figs. 4a and 4b, $\boldsymbol{r}_j^I = \boldsymbol{T}_j^{-1} \cdot (\xi_j, \eta_j, 0)^T + \boldsymbol{r}_{ac,j} = \boldsymbol{r}_j^A + \boldsymbol{T}_j^{-1} \cdot (\xi_j, 0, 0)^T = \boldsymbol{T}_j^{-1} \cdot (\xi_j, \eta_j, 0)^T + (x_{ac,j}, 0, 0)^T$. When a solid body motion ($\ddot{\boldsymbol{r}}_j^I = 0$) is assumed, the inertial force and moment are, respectively, given by

$$\boldsymbol{F}^I = \sum_{j=1}^n \iint \boldsymbol{a}_j \left(\frac{d^2m}{d\xi\,d\eta} \right) d\xi\,d\eta = -m(\dot{\boldsymbol{u}} + \boldsymbol{\omega} \times \boldsymbol{u}) \quad (14a)$$

$$\boldsymbol{M}^I = -\sum_{j=1}^n \iint \boldsymbol{r}_j^I \times \boldsymbol{a}_j \left(\frac{d^2m}{d\xi\,d\eta} \right) d\xi\,d\eta = -\boldsymbol{J} \cdot \dot{\boldsymbol{\omega}} - \boldsymbol{\omega} \times \boldsymbol{J} \cdot \boldsymbol{\omega}$$

$$(14b)$$

where

$$\sum_{j=1}^n \iint \boldsymbol{r}_j^I \left(\frac{d^2m}{d\xi\,d\eta} \right) d\xi\,d\eta = 0$$

$\boldsymbol{J}$ is the inertial tensor, and where the integration should be performed over the entire area of the jth blade, and the summation must cover all blades.

Because the origin of the body coordinate system is located at the c.g. of the boomerang, the following relations are established:

$$\sum_{j=1}^n (x_{ac,j} + \bar{\xi} \sin \Lambda_j + \bar{\eta} \cos \Lambda_j) = 0$$

$$\sum_{j=1}^n (-\bar{\xi} \cos \Lambda_j + \bar{\eta} \sin \Lambda_j) = 0$$

a) Position of a blade element

b) Inertial force acting on a blade element ($\Delta\theta_t = 0$)
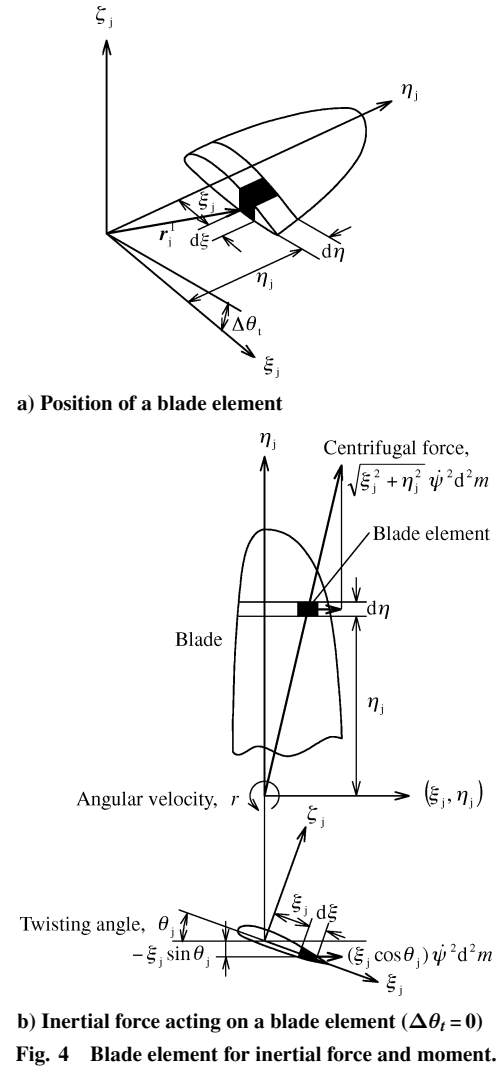
Fig. 4   Blade element for inertial force and moment.

Equations of Motion

The equations of motion of a boomerang assumed to be a rigid body can be derived by summing the aerodynamic, gravity, and inertial forces and their moments as follows:

$$\boldsymbol{F}^A + \boldsymbol{F}^G + \boldsymbol{F}^I = 0 \qquad (15a)$$

or

$$m \begin{pmatrix} \dot{u}_x + qu_z - ru_y \\ \dot{u}_y + ru_x - pu_z \\ \dot{u}_z + pu_y - qu_x \end{pmatrix} = \frac{1}{2}\rho(R\Omega)^2 S \begin{pmatrix} C_x^A \\ C_y^A \\ C_z^A \end{pmatrix} - mg \begin{pmatrix} C_x^G \\ C_y^G \\ C_z^G \end{pmatrix}$$

$$(15b)$$

$$\boldsymbol{M}^A + \boldsymbol{M}^G + \boldsymbol{M}^I = 0 \qquad (16a)$$

or

$$\begin{pmatrix} (I_x\dot{p} - J_{xy}\dot{q} - J_{xz}\dot{r}) + (I_z - I_y)qr + (J_{xy}p + J_{yz}r)r - (J_{xz}p + J_{yz}q)q \\ (I_y\dot{q} - J_{yz}\dot{r} - J_{xy}\dot{p}) + (I_x - I_z)pr + (J_{yz}q + J_{xz}p)p - (J_{xy}p + J_{xz}r)r \\ (I_z\dot{r} - J_{xz}\dot{p} - J_{yz}\dot{q}) + (I_y - I_x)pq + (J_{xz}r + J_{xy}q)q - (J_{yz}r + J_{xy}p)p \end{pmatrix} = \frac{1}{2}\rho(R\Omega)^2 RS \begin{pmatrix} C_{M,x}^A \\ C_{M,y}^A \\ C_{M,z}^A \end{pmatrix} \quad (16b)$$

The geometrical configurations of the respective blades are prescribed, and thus, the moments and products of inertia, $I_{\xi,j}$, $I_{\eta,j}$, and $J_{\xi\eta,j}$, and the coning and sweep angles β_j and Λ_j are also known previously.

where R and S are reference radius and area, respectively, and Ω is the angular velocity about z axis or spin rate at the initial state,

$$\Omega = \dot{\psi}(t = 0) = r(t = 0) \qquad (17)$$

The detailed expression of the aerodynamic and gravity force coefficients, and the aerodynamic moment coefficient, are given as follows.

Aerodynamic force coefficients:

$$C_x^A = \sum_{j=1}^n \int_0^{R_j/R} \left[\frac{w^2 cR}{\{(R\Omega)^2 S\}} \right] [(-C_\ell \sin\alpha + kC_d \cos\alpha) \sin\Lambda$$

$$+ (\theta \sin\Lambda - \beta \cos\Lambda)(C_\ell \cos\alpha + kC_d \sin\alpha)]_j \, d\left(\frac{\eta}{R}\right)$$

$$= \sum_j C_{x,j}^A \tag{18a}$$

$$C_y^A = \sum_{j=1}^n \int_0^{R_j/R} \left[\frac{w^2 cR}{\{(R\Omega)^2 S\}} \right] [-(-C_\ell \sin\alpha + kC_d \cos\alpha) \cos\Lambda$$

$$- (\theta \cos\Lambda + \beta \sin\Lambda)(C_\ell \cos\alpha + kC_d \sin\alpha)]_j \, d\left(\frac{\eta}{R}\right)$$

$$= \sum_j C_{y,j}^A \tag{18b}$$

$$C_z^A = \sum_{j=1}^n \int_0^{R_j/R} \left[\frac{w^2 cR}{\{(R\Omega)^2 S\}} \right] [-\theta(-C_\ell \sin\alpha + kC_d \cos\alpha)$$

$$+ (C_\ell \cos\alpha + kC_d \sin\alpha)]_j \, d\left(\frac{\eta}{R}\right) = \sum_j C_{z,j}^A \tag{18c}$$

Aerodynamic moment coefficients:

$$C_{M,x}^A = \sum_{j=1}^n \int_0^{R_j/R} \left[\frac{w^2 cR}{\{(R\Omega)^2 S\}} \right] \left[(C_l \sin\alpha + kC_d \cos\alpha)\left(\frac{\eta}{R}\right) \sin\Lambda \right.$$

$$- (\theta \sin\Lambda - \beta \cos\Lambda)(-C_\ell \cos\alpha + kC_d \sin\alpha)\left(\frac{\eta}{R}\right)$$

$$\left. + \left(\frac{c}{R}\right)C_m \cos\Lambda \right]_j d\left(\frac{\eta}{R}\right) \tag{19a}$$

$$C_{M,y}^A = \sum_{j=1}^n \int_0^{R_j/R} \left[\frac{w^2 cR}{\{(R\Omega)^2 S\}} \right]$$

$$\times \left[-(C_\ell \sin\alpha + kC_d \cos\alpha)\left(\frac{\eta}{R}\right)\cos\Lambda \right.$$

$$+ (\theta \cos\Lambda + \beta \sin\Lambda)(-C_\ell \cos\alpha + kC_d \sin\alpha)\left(\frac{\eta}{R}\right)$$

$$\left. - \left(\frac{c}{R}\right)C_m \cos\Lambda \right]_j d\left(\frac{\eta}{R}\right) - \sum_j \left\{ \left(\frac{x_{ac,j}}{R}\right)C_{z,j}^A \right\} \tag{19b}$$

$$C_{M,z}^A = \sum_{j=1}^n \int_0^{R_j/R} \left[\frac{w^2 cR}{\{(R\Omega)^2 S\}} \right] \left[-\theta(C_\ell \cos\alpha + kC_d \sin\alpha)\left(\frac{\eta}{R}\right) \right.$$

$$- (-C_l \cos\alpha + kC_d \sin\alpha)\left(\frac{\eta}{R}\right)$$

$$\left. + \left(\frac{c}{R}\right)C_m \cos\Lambda \right]_j d\left(\frac{\eta}{R}\right) + \sum_j \left\{ \left(\frac{x_{ac,j}}{R}\right)C_{y,j}^A \right\} \tag{19c}$$

Gravity force coefficients:

$$C_x^G = -(\cos\theta \cos\psi) \sin\Theta_0 + (\cos\theta \sin\psi) \sin\Phi_0 \cos\Theta_0$$

$$- (\sin\theta) \cos\Phi_0 \cos\Theta_0 \tag{20a}$$

$$C_y^G = (\cos\phi \sin\psi - \sin\phi \sin\theta \cos\psi) \sin\Theta_0$$

$$+ (\cos\phi \cos\psi + \sin\phi \sin\theta \sin\psi) \sin\Phi_0 \cos\Theta_0$$

$$+ (\sin\phi \cos\theta) \cos\Phi_0 \cos\Theta_0 \tag{20b}$$

$$C_z^G = -(\sin\phi \sin\psi + \cos\phi \sin\theta \cos\psi) \sin\Theta_0$$

$$- (\sin\phi \cos\psi - \cos\phi \sin\theta \sin\psi) \sin\Phi_0 \cos\Theta_0$$

$$+ (\cos\phi \cos\theta) \cos\Phi_0 \cos\Theta_0 \tag{20c}$$

Note that these coefficients are functions of time.

The six Eqs. (15) and (16) can be solved for six unknown variables: velocity $u = (u_x, u_y, u_z)^T$ and Euler's angles $(\psi, \theta, \phi)^T$ as functions of an independent variable, time t. The initial conditions are given by $u_0 = (u_x, u_y, u_z)_0^T$, $(\dot\psi, \dot\theta, \dot\phi)_0^T$ and $(\psi, \theta, \phi)_0^T$. The orientation of the nonslipping or nonspinning frame defined by Euler's angles Ψ, Θ, and Φ can be obtained by integrating Eqs. (6d–6f) with the initial condition given by $(\Psi, \Theta, \Phi)_0^T$.

The position vector of the origin of the body frame or nonspinning frame $R = (X, Y, Z)^T$ is obtained by integrating the velocity U specified by Eq. (7b) with the initial condition of $R_0 = (X, Y, Z)_0^T$ as follows:

$$R = \int_0^t U \, dt + R_0 \tag{21}$$

Energy

The total energy E of a boomerang can be given by

$$E = \tfrac{1}{2}mu^2 + mgZ + \tfrac{1}{2}\omega \cdot J \cdot \omega = E^L + E^P + E^R \tag{22}$$

where $E^L = \tfrac{1}{2}mu^2$, $E^P = mgZ$, and $E^R = \tfrac{1}{2}\omega \cdot J \cdot \omega$ and where Z is the altitude of the boomerang in flight,

$$Z = \int_0^t u \cdot T \cdot (T_I)_0 \cdot K_I \, dt + Z_0 \tag{23}$$

Typical Round-Trip Flight

In this section, numerical calculations are performed to analyze the fundamental characteristics of the flight of a two-bladed and symmetrically arranged boomerang after being launched by hand.

Aerodynamic Coefficients of a Blade Element

Numerical analyses and experimental tests were conducted only for a two-bladed aboriginal boomerang. Here, the boomerang is assumed to be symmetric with respect to the (x, y) plane and to have been thrown by the right hand. The detailed geometrical configurations of the exemplified boomerang are given in Table 1.

The tip speed $R\Omega$ of a boomerang is much lower than a helicopter rotor, such that the advance ratio $\mu = w_X/R\Omega$ and the inflow ratio $\bar\lambda = w_Z/R\Omega$ of a blade element (an airfoil at any spanwise station) are very high in comparison with those of a helicopter rotor. Thus from T_n in Table 1, the relative velocity components are given by $w_X = w_x \cos\lambda - w_y \sin\lambda$, $w_Y = w_x \sin\lambda + w_y \cos\lambda$, and $w_Z = w_z$. Then, the ranges of the reversed flow region and of the high angle of attack beyond the stall limit of the airfoil occupy very wide areas of the blade rotational plane.

Thus, aerodynamic coefficients of the airfoil must be known for the full range of angle of attack. With reference to the aerodynamic characteristics of NACA 0012 and 0015 at Reynolds number $Re = (0.5 \sim 1.8) \times 10^6$ (Refs. 5–8) and wind-tunnel tests conducted at Tokai University,[9] the aerodynamic coefficients presented in Fig. 5 were assumed applicable to the present numerical

analysis. The mean Reynolds number at spanwise station $\eta_j = \frac{3}{4}\ell_j$ is $Re = 5.5 \times 10^4$ for the present study. Note that the directions of positive drag, lift, and moment are defined, respectively, as follows: The drag is parallel to the relative velocity $(w_\xi, 0, w_\eta)^T$, the lift is normal to both the foregoing relative velocity and a spanwise unit vector along the feathering axis $\boldsymbol{\eta}$ or parallel to their vector product $(w_\xi, 0, w_\eta)^T \times \boldsymbol{\eta}$, and the moment is defined to act about the spanwise vector $\boldsymbol{\eta}$.

Example of Flight

Equations of motion given by Eqs. (15) and (16) are solved numerically by the Runge–Kutta method (see Kreyszig[10]) with the time increment of $\Delta t = 1.66 \times 10^{-4} \sim 1.00 \times 10^{-5}$ s. The flight path or the excursion of the c.g. is shown projected on (X_I, Y_I) (Fig. 6a), (X_I, Z_I) (Fig. 6b), and (Y_I, Z_I) (Fig. 6c), planes. Because the initial yawing angle is taken to be $\Psi_0 = 45$ deg, the longitudinal and lateral distances from an initial point are determined by Y_I and X_I,

respectively. Open circles represent every 5 rotations or spins of the boomerang, and numerals are affixed for every 5 rotations. It can be seen that, as well known, a boomerang or specifically a returning boomerang, returns to some area close to the place where it was released after having made a round-trip of counter-clockwise route in the (X_I, Y_I) plane for a right-handed throw, accompanied by some altitude and speed changes. Time histories of flight distance (Fig. 6d) from the initial takeoff point $|\boldsymbol{R} - \boldsymbol{R}_0|$, altitude Z (Fig. 6e), and flight speed $|\boldsymbol{U}| = |\boldsymbol{u}| = U$ (Fig. 6f) are also shown. It is clear that the exemplified boomerang thrown with an adequate set of speed and spin rate completes the round-trip in several seconds, encircling a diameter of about 15 m and reaching a maximum altitude of about 5 m.

Fig. 5   Two-dimensional aerodynamic characteristics used for numerical analysis.

Table 1   Geometrical dimension of an exemplified boomerang for numerical calculations

| Parameter	Value
Length of one blade ℓ, m	3.00×10^{-1}
Radius of rotation R, m	2.69×10^{-1}
Blade area, S_b, m^2	2.76×10^{-2}
Mean chord $\bar{c}$, m	4.88×10^{-2}
Disk area S, m^2	2.28×10^{-1}
Mass m, kg	1.30×10^{-1}
Position of a.c. x_{ac}, m	7.23×10^{-2}
Center of gravity $\bar{\xi}$, m	0.00
$\bar{\eta}$, m	1.45×10^{-1}
Sweep angle Λ_1, deg	120
Λ_2, deg	240
Folding angle γ, deg	120
Coning angle β, deg	0.00
Pitching angle θ, deg	0.00
Moment of inertia I_ξ, kg·m^2	1.90×10^{-3}
I_η, kg·m^2	4.88×10^{-6}
I_ς kg·m^2	1.90×10^{-3}
Product of inertia $J_{\xi\eta}$, kg·m^2	5.14×10^{-21}
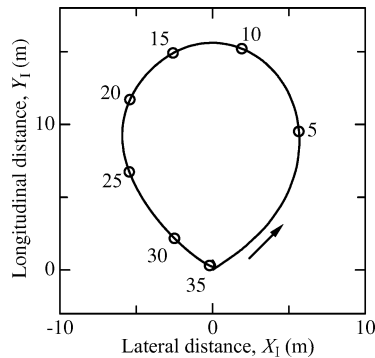
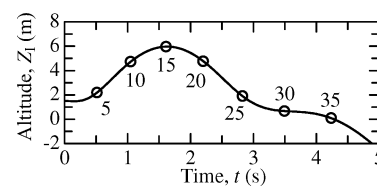a) (X_I, Y_I) plane
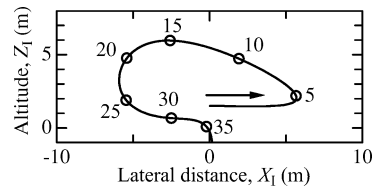
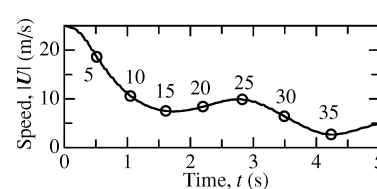b) (X_I, Z_I) plane
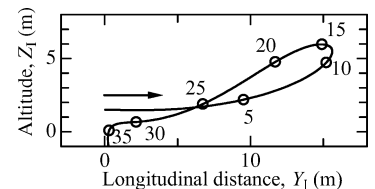
c) (Y_I, Z_I) plane
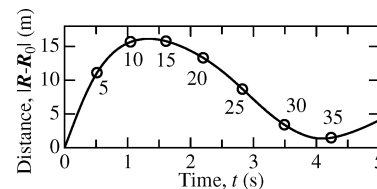
d) **Distance from initial point**

e) **Altitude**

f) **Speed**

Fig. 6   Time history of the flight of a representative boomerang: $U_0 = 25$ m/s, $r_0 = 10$ Hz, and $\Phi_0 = 70$ deg (numbers show number of spins).
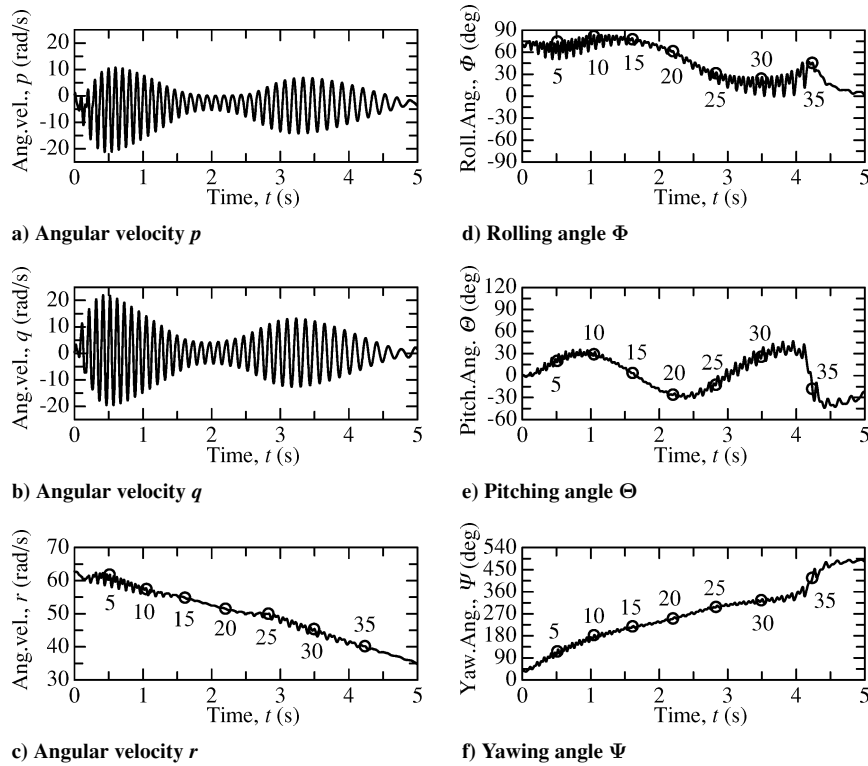
Fig. 7   Time history of angular velocity and Euler's angle of a representative boomerang.
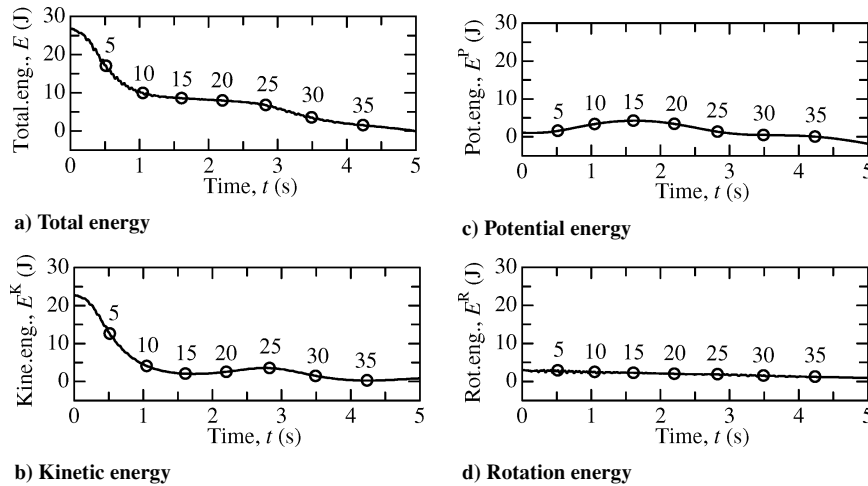

Fig. 8   Time history of the energy of a representative boomerang.

Figures 7a–7c and 7d–7f show, respectively, the angular velocity components of the body-fixed frame and Euler's angles (Ψ, Θ, Φ) of the nonspinning frame. Obviously, a short-period oscillation (Figs. 7a and 7b), the frequency of which coincides with that of spin about z axis of one blade, is observed with strong pitching and rolling motions. The amplitude of this oscillation increases in ascending flight path ($t = 0.5$–1.5 s) and decreases in descending flight path ($t = 1.5$–2.5 s). The oscillation can also be observed in Euler's angles of the nonspinning frame with twice the frequency.

Figure 8a shows the total energy E; Fig. 8b the kinetic energy E^K, consisting of linear and rotational energies, E^L and E^R; Fig. 8c the potential energy E^P; and Fig. 8d the rotation energy E^R. It is interesting to find that 1) the boomerang has a kind of damped phugoid oscillation, which shows a slow interchange between kinetic and potential energies (Figs. 8b and 8c) and 2) although the linear kinetic energy and the potential energy decrease as the time elapses, the spin rate about the z axis and, thus, the rotational energy, does not decrease as much. The change of the total energy comes mainly from

the change of the kinetic and potential energies. The contribution of the change of the rotation energy is small. The reduction of the spin rate about the z axis is slightly flattened between the 10th and 25th spin, as shown in Fig. 7c, because of the autorotation effect caused by the upward inflow $U_p = V \sin(\Theta - \gamma) - \bar{v}$ along the z axis due to either the forward speed with the positive pitch angle of the apparent disk (the rotational plane of the blades) $\Theta > 0$ or the descent flight ($\gamma < 0$) with near zero pitch angle $\Theta = 0$. Then the driving force for the rotation comes from the upward inflow $U_p > 0$, which can be obtained even in climbing flight if $U_p = V \sin(\Theta - \gamma) - \bar{v} > 0$, like the climbing flight of an autogyro the rotor speed of which is kept constant due to high tiltback angle $\Theta > \gamma + \sin^{-1}(\bar{v}/V)$.

When the flight paths shown in Figs. 6–8 are divided into four chronological blocks after takeoff, the following phenomena can also be observed.

First, in the first block up to about the 15th rotation, although the speed of the boomerang decreases gradually, the spin rate is still high enough for the boomerang to take an upward- and leftward-curved
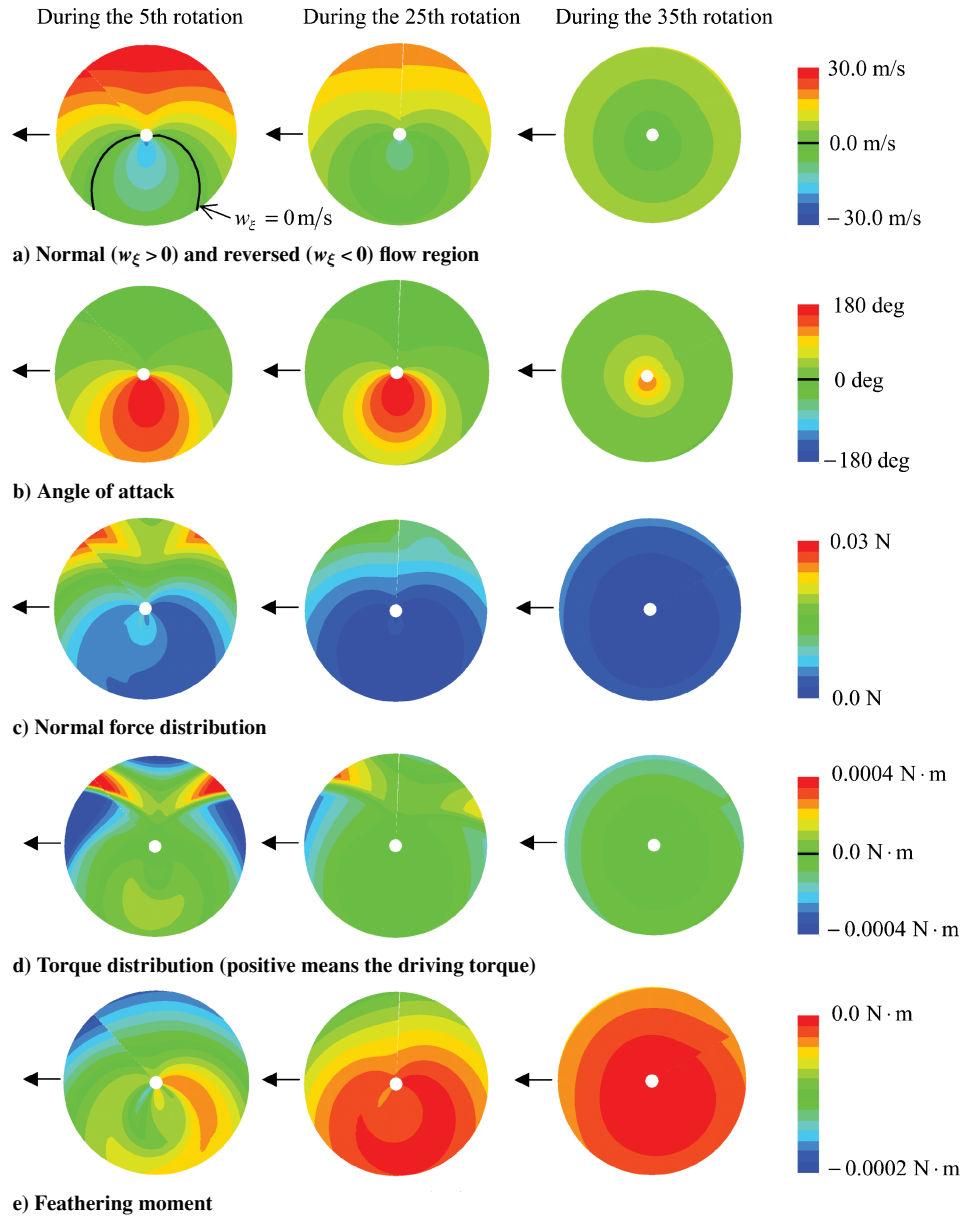
During the 5th rotation   During the 25th rotation   During the 35th rotation

30.0 m/s

0.0 m/s

−30.0 m/s

a) Normal ($w_\xi > 0$) and reversed ($w_\xi < 0$) flow region

180 deg

0 deg

−180 deg

b) Angle of attack

0.03 N

0.0 N

c) Normal force distribution

0.0004 N · m

0.0 N · m

−0.0004 N · m

d) Torque distribution (positive means the driving torque)

0.0 N · m

−0.0002 N · m

e) Feathering moment

Fig. 9   Variations of physical quantities observed in nonspinning frame.

path. The distance from the takeoff point $|\boldsymbol{R} - \boldsymbol{R}_0|$ and the altitude Z increase and attain their maximum values. The flight speed decreases and reaches its local minimum value. The rolling angle Φ slightly decreases first and then increases, whereas the pitching angle Θ slightly increases and falls back again. The reduction of the spin rate about z axis and, thus, of the rotational energy E^R itself is large except the earlier specified range (20th–25th rotation), but its contribution to the total energy E is small, as shown in Fig. 8d.

Figures 9a and 9b show the reversed flow region ($w_\xi < 0$) and the angle-of-attack distribution observed during the 5th (left), 25th (middle), and 35th (right) rotations, respectively. In Fig. 9 drawn in the rotational plane, the circle centers coincide with the origin of the coordinate system (ξ_j, $\boldsymbol{\eta}_j$, ζ_j) of any one of the blades, and thus, any aerodynamic quantity is represented by a position specified by radius η_j and azimuth angle ψ on the line of the a.c., which, as seen from Fig. 2, does not pass through the c.g. of the boomerang. Following the first blade, the second blade traces the same circumstance with the phase lag of ($\pi - \gamma$).

In the early stage, the regions of reversed flow and the high angle of attack can be observed mainly near the three-quarter azimuth angle. Because the origin of the circle does not coincide with the c.g., the boundary of the reversed flow ($w_\xi = 0$) does not coincide

with a circle. The size of both regions decreases as time elapses because the advance ratio decreases with time and disappears near the hovering flight.

As stated earlier, in the middle part of this chronological block, a marked short-period oscillation is observable. This is, as shown in Fig. 9c, mainly generated by an unbalanced normal force or lift distribution between the first and second blades. The high lift is obtained during the first rotation near tip side of the blade in its first quarter for the first blade and the low lift in the third quarter for the second blade.

Second, in the second chronological block from the 15th to the 25th rotations, after reaching the maximum altitude, the boomerang begins to take a returning path. The altitude Z decreases and approaches its local minimum value, and thus, the speed U and the kinetic energy E^K reach the local maximum value. The rolling angle Φ decreases appreciably, whereas the pitching angle Θ oscillates up and down. During the flight in this block, the short-period oscillation is very small and the spin rate r decreases slightly.

Third, in the third chronological block from the 25th to the 35th rotations, the boomerang takes a direct returning course toward the initial takeoff point $\boldsymbol{R}_0$. Because the pitching angle Θ in the latter

half increases to apply a breaking action, the flight speed decreases. However, the flight altitude is kept almost constant, and it is nearly the same level as the initial altitude $Z \cong Z_0$. In this block, the marked short-period oscillation is observed again due to the reversed and stalled flow regions and the unbalanced lift distribution. Near the 35th rotation, the boomerang's yawing angle increases to more than 360 deg, and the boomerang attains nearly the local maximum values of rolling attitude and its altitude, while its flight speed reaches the local minimum value. As can be seen from Figs. 9a–9c, these features result from the homogeneous flow and force distributions in a near hovering flight. Then, a human hand can easily catch the boomerang.

Fourth, in the final chronological block beyond the 35th rotation, after having passed the nearest point to the site of initial takeoff, and making a short, near hovering flight, the boomerang loses altitude and makes a soft landing. Because of the low forward speed, the relative speed and angle-of-attack distribution are homogeneous over the rotational plane.

Figures 9d and 9e show the torque and feathering moment distributions observed in the rotational plane, respectively. The torque is relatively large at the 5th rotation on the right-hand side before and behind the azimuth angle of $\psi = 90$ deg, but it is very homogeneous and close to zero at the 35th rotation. The feathering moment at the 5th rotation is negatively large at $\psi = 90$ deg, but the feathering moment at the 35th rotation is nearly zero and homogeneous.

Conclusions

Precise equations of motion for solving the flight dynamics of a boomerang were established and solved numerically for a returning boomerang. The solution shows that the motion consists of both long- and short-period oscillations. The long-period oscillation originates from the exchange of potential energy with kinetic energy, mainly derived 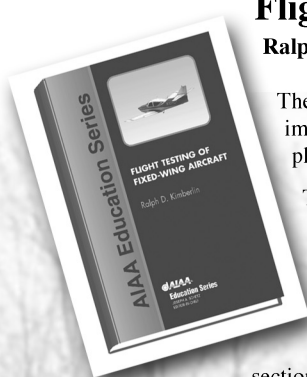from the forward motion and the spinning motion, the latter of which decreases slightly by the autorotation when the angle of attack of an apparent disk of blade rotation increases. The short-period oscillation is due to an asymmetry in the aerodynamic moment related to a large reversed-flow region due to high-advance-ratio flight and a large moment of inertia. The returning flight is realized by the centripetal component of the aerodynamic force acting on the apparent disk, which is tilted inwardly from the described asymmetric moment and the resulting gyro effect of the spinning motion.

References

[1]Hess, F., "The Aerodynamics of Boomerangs," *Scientific American*, Vol. 29, No. 5, 1968, pp. 124–136.

[2]Hess, F., *Boomerangs, Aerodynamics and Motion*, Rijksuniversiteit Te Groningen, Groningen, The Netherlands, 1975.

[3]King, A. L., "Project Boomerang," *America Journal of Physics*, Vol. 43, No. 9, 1975, pp. 770–773.

[4]Vos, H., "Straight Boomerang of Balsa Wood and Its Physics," *America Journal of Physics*, Vol. 53, No. 6, 1985, pp. 524–527.

[5]Critzos, C. C., Heyson, H. H., and Boswinkle, R. W., Jr., "Aerodynamic Characteristics of NACA 0012 Airfoil Section at Angles of Attack from $0°$ to $180°$," NACA TN-3361, Jan. 1955.

[6]Pope, A., and Harper, J. J., *Low-Speed Wind Tunnel Testing*, Wiley, New York, 1966, Chap. 7.

[7]Gessow, A., and Crim, A. D., "A Method for Studying the Transient Blade-Flapping Behavior of Lifting Rotors at Extreme Operating Conditions," NACA TN-3366, 1955.

[8]Gessow, A., and Tapscott, R. J., "Charts for Estimating Performance of High-Performance Helicopters," NACA Rept. 1266, Jan. 1956; supersedes NACA TN-3323, and -3482, 1955.

[9]Ishikawa, H., Beppu, G., and Azuma, A., "An Analysis of Boomerang's Flight Dynamics," *Proceedings of 4th Sky Sports Symposium*, Japan Society for Aeronautical and Space Sciences, Tokyo, 1998, pp. 69–72.

[10]Kreyszig, E., *Advanced Engineering Mathematics*, 8th ed., Wiley, New York, 1999, Chap. 19.